Supporting Information

Atomic cation and anion co-vacancy defects boosted the oxide path mechanism of oxygen evolution reaction on NiFeAl-layered double hydroxide

Zhaoyan Li[1], Duo Wang[2], Hongguang Kang[2], Zhongning Shi[2], Xianwei Hu[2], Hongbin Sun[1], Junli Xu[1]*

1- College of Science, Northeastern University, Shenyang, 110819, Liaoning, China

2- Key Laboratory for Ecological Metallurgy of Multimetallic Mineral (Ministry of Education), Northeastern University, Shenyang, 110819, Liaoning, China

*- Corresponding author. E-mail address: jlxu@mail.neu.edu.cn (J. Xu).

Experimental section

Chemicals and reagents

Ni foam (1 cm × 3 cm), $Ni(NO_3)_2·6H_2O$ (≥98.0%), $Fe(NO_3)_3·9H_2O$ (98.5~101.0%), $Al(NO_3)_3·9H_2O$ (99.99%), $CO(NH_2)_2$ (≥99.0%), NH_4F (≥96.0%), HCl (37.0~38.0%), KOH (≥85.0%) and CH_3CH_2OH (≥99.7%) were utilized for synthesis and all used as received.

Synthesis of $Ni_6Fe_2Al_x$-LDH

$Ni_6Fe_2Al_x$-LDH (x = 0.5, 1, 2) nanosheets were in situ growth on nickel foam (NF) through a hydrothermal reaction. Specifically, a piece of NF was first ultrasonicated with 3 mol L^{-1} HCl and then washed with ethanol and deionized (DI) water to clean its surface. Subsequently, it was put into a 100 mL Teflon-line stainless-steel autoclave containing a mixed solution of 2.25 mmol $Ni(NO_3)_2·6H_2O$, 0.75mmol $Fe(NO_3)_3·9H_2O$, n mmol $Al(NO_3)_3·9H_2O$ (n = 0.1875, 0.375, 0.75), 15 mmol $CO(NH_2)_2$ and 15 mmol NH_4F, and maintained at 120 ℃ for 12 h. After cooling to room temperature, the NF with $Ni_6Fe_2Al_x$-LDH nanosheets on its surface was taken out, rinsed several times, and dried in an electric oven at 60 ℃.

Synthesis of C-$Ni_6Fe_2Al_x$-LDH

The cationic vacancy defected $Ni_6Fe_2Al_x$-LDH (C-$Ni_6Fe_2Al_x$-LDH) was prepared by a alkaline corrosion reaction. Briefly, the obtained $Ni_6Fe_2Al_x$-LDH was immersed in a 6 mol L^{-1} KOH for 3h at 60 ℃. After the reaction was completed, the resulting C-$Ni_6Fe_2Al_x$-LDH sample was washed with DI water three times to remove surface impurities.

Synthesis of CR-$Ni_6Fe_2Al_x$-LDH

The co-vacancy defected $Ni_6Fe_2Al_x$-LDH (CR-$Ni_6Fe_2Al_x$-LDH) was synthesized by a electrochemical reduction method. In detail, the prepared C-$Ni_6Fe_2Al_x$-LDH, platinum

sheet and Hg/HgO were used as working electrode, counter electrode and reference electrode. In 1 mol L^{-1} KOH, cyclic voltammetry was carried out, working potential range was 0 ~ -1.3 V and CV cycle 5 circles at 5 mV s^{-1}.

Materials characterization

The surface chemical compositions and valence states of the resulting samples were determined by X-ray diffractometer (XRD, Empyrean type instrument manufactured by PANalytical, Cu Kα radiation) and X-ray photoelectron spectroscopy (XPS, Thermo Scientific ESCALAB Xi+). The morphologies and elemental analysis of these catalysts were investigated using scanning electron microscopy (SEM) and energy dispersive spectroscopy (EDS) attached to the SEM (Hitachi SU8010). The specific microstructural information was obtained by transmission electron microscopy (TEM, FEI Talos F200x) and atomic force microscopy (AFM, Bruker Dimension Icon). The formation of oxygen and cation vacancies was certified by electron spin resonance (ESR, Bruker A300). The metal content of prepared catalysts was obtained from atomic absorption spectrometer (AAS, AAS6000). Raman spectra were collected using a high speed and high resolution confocal Raman spectrometer (LabRAM Odyssey^{TM}) with an excitation wavelength of 532 nm and a 50× objective. The Ni, Fe, Al content of CR-Ni_6Fe_2Al-LDH and KOH solution after stability test were tested by inductively coupled plasma optical emission spectrometer (ICP-OES, ThermoICPOES7200) using nitrogen as the carrier gas.

Electrochemical measurements

A typical three-electrode system in 1 mol L^{-1} KOH was utilized to measure the electrochemical performance by a CHI 660E electrochemical workstation, which comprised of a working electrode (prepared catalysts), counter electrode (platinum

sheet) and reference electrode (Hg/HgO). All the tested potentials vs. Hg/HgO were calibrated to potentials vs. RHE via the equation:

$$E_{RHE} = E_{Hg/HgO} + 0.0592\ pH + 0.098 \qquad (1)$$

The OER activity was evaluated via using linear sweep voltammetry (LSV, scan rate: 5 mV/s) with 90% iR compensation. The conductivity was estimated by utilizing electrochemical impedance spectroscopy (EIS) within a 10^5 Hz - 10^{-1} Hz frequency range at 1.56 V vs. RHE. The double-layer capacitance (C_{dl}) was gained by cyclic voltammetry (CV) method at scan rates from 20 to 120 mV s^{-1}. Typically, the potentials were swept between 0.93 V_{RHE} and 1.03 V_{RHE}. The long-term stability was tested at 200 mA cm^{-2} for 100 h.

The TOF values was calculated by the following formula:

$$TOF = \frac{\mathrm{j} \times A}{4 \times \mathrm{n} \times F} \qquad (2)$$

Where j is the current density at a given overpotential based on the LSV curves, A is the geometric surface area of working electrode (1 cm^2 in this work), F is the Faraday constant (96485 C mol^{-1}), and n is the number of moles of active materials on the working electrode (Based on all metal content were obtained from AAS results).

The semiconductor type of the material and the change in carrier concentration after the introduction of defects were determined by the Mott-Schottky (MS) analysis. The synthesized catalysts, platinum sheet and Ag/AgCl were used as the working electrode, the counter electrode and the reference electrode, respectively. The MS test was carried out in a potential range from -0.1 to 1.3 V vs. Ag/AgCl, the amplitude and the frequency were set as 0.01 V and 10^3 Hz in 0.5 mol L^{-1} Na_2SO_4. The relationship between the measured capacitance and voltage was described by the equation:

$$\frac{1}{C^2} = -\frac{2}{\varepsilon_0 \varepsilon\, \mathrm{e}\, N}\left(E - E_{\mathrm{fb}} - \frac{KT}{\mathrm{e}}\right) \qquad (3)$$

where C is the capacitance, E is the voltage, ε_0 is the vacuum permittivity, ε is the relative permittivity of the material, e is the fundamental charge, N is the carrier concentration, K is Boltzmann's constant, T is the temperature and E_{fb} is the flat band potential. Based on this relationship, N is inversely proportional to the slope of the Mott-Schottky plot.

The electrochemical activation energy (E_a, kJ mol^{-1}) for OER was calculated through the Arrhenius relationship below:

$$\log j = -\frac{E_a}{2.303RT} + C \qquad (4)$$

where j represents the current density (mA cm^{-2}) at a given potential, R is the gas constant (8.314 J K^{-1} mol^{-1}), T is the temperature (K) and C is a constant.

Theoretical calculation methods

First-principles calculations of density functional theory (DFT) were performed based on plane wave pseudopotential through the CASTEP module of Materials studio (MS) commercial software. The ultra-soft pseudopotential was used to describe the interaction between ionic cores and valence electrons. The exchange correlation energy was calculated by the generalized gradient approximation (GGA) of the Perdew-Burke-Ernzerhof (PBE) function. The convergence criteria for the optimization of the architecture were as follows: the cutoff energy for the plane-wave basis was set to 550 eV. The convergence threshold of the total ionic relaxation energy was converged to 10^{-5} eV, and 0.01 eV/Å for force. The k-point meshes were selected as 5×5×1. A 20 Å vacuum layer was used to eliminate the electrostatic interactions. Furthermore, the spin polarization of the electron was fully considered for this calculation.

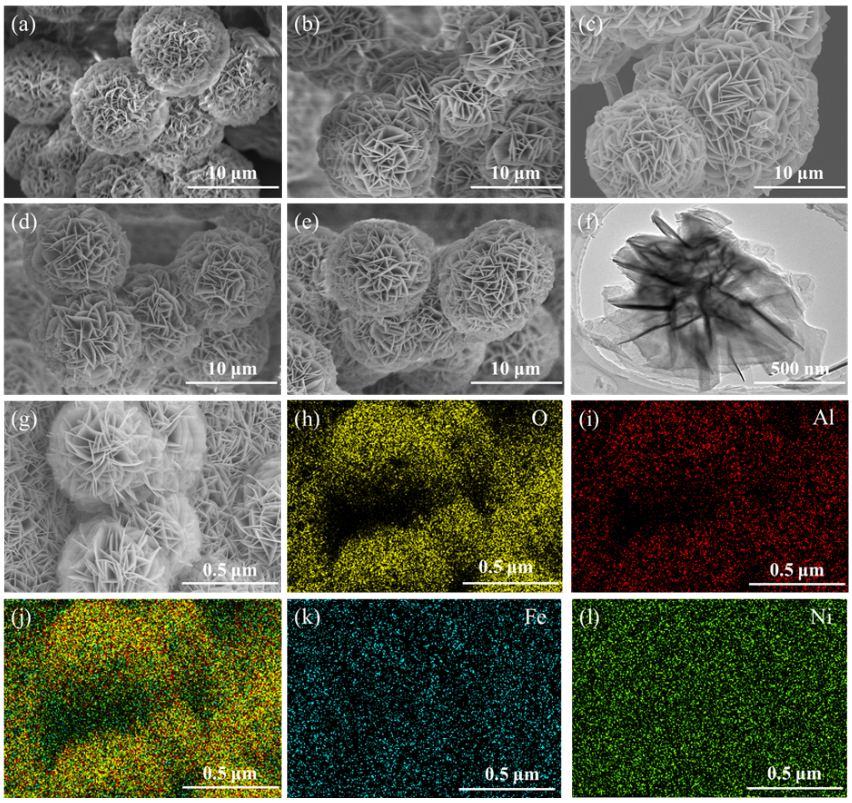

Fig. S1. SEM, TEM and mapping images of prepared samples. (a-f) Ni_6Fe_2Al-LDH (a), C-Ni_6Fe_2Al-LDH (b), CR-Ni_6Fe_2Al-LDH (c), CR-$Ni_6Fe_2Al_{0.5}$-LDH (d), CR-$Ni_6Fe_2Al_2$-LDH (e), and TEM image (f) of CR-Ni_6Fe_2Al-LDH. (g-l) SEM image and the corresponding elemental mapping.

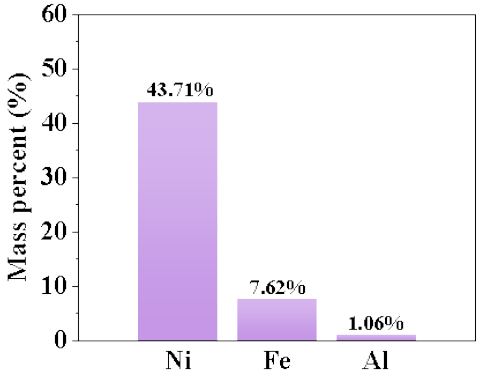

Fig. S2. The mass percent of Ni, Fe, Al in CR-Ni_6Fe_2Al-LDH determined by ICP-OES measurement.

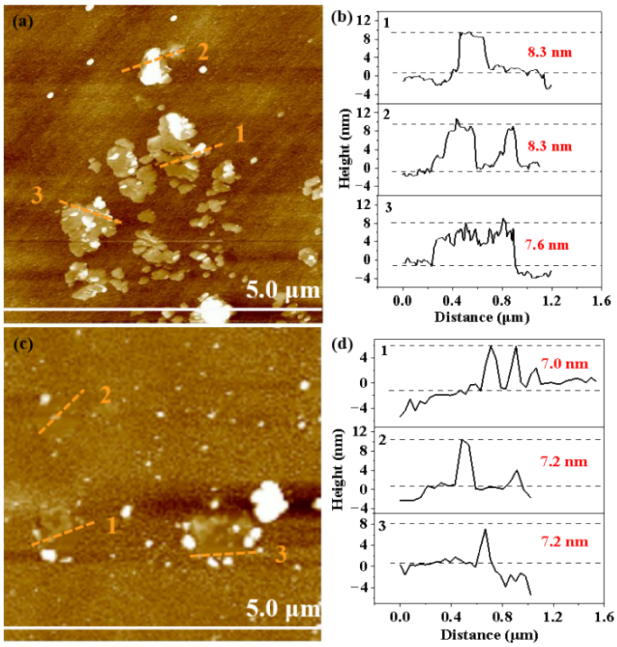

Fig. S3. AFM images of prepared samples. (a, b) Ni_6Fe_2Al-LDH. (c, d) C-Ni_6Fe_2Al-LDH.

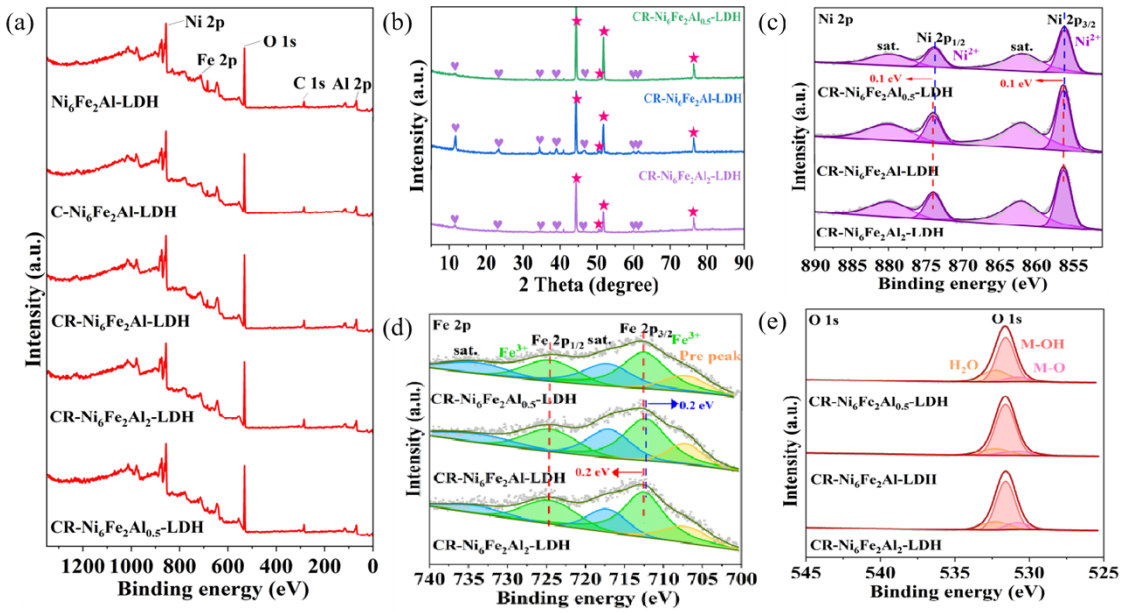

Fig. S4. XPS spectra and XRD patterns of prepared samples. (a) XPS survey spectra of Ni_6Fe_2Al-LDH, C-Ni_6Fe_2Al-LDH, CR-Ni_6Fe_2Alx-LDH (x=0.5, 1 and 2). (b-e) XRD patterns (b), Ni 2p (c), Fe 2p (d), and O 1s spectra (e) of CR-Ni_6Fe_2Alx-LDH (x=0.5, 1 and 2).

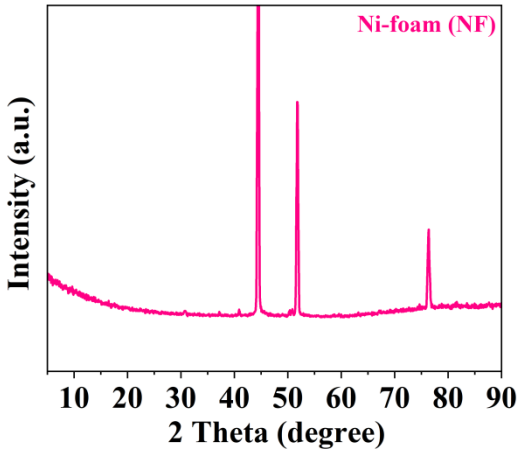

Fig. S5. XRD patterns of Ni-foam (NF).

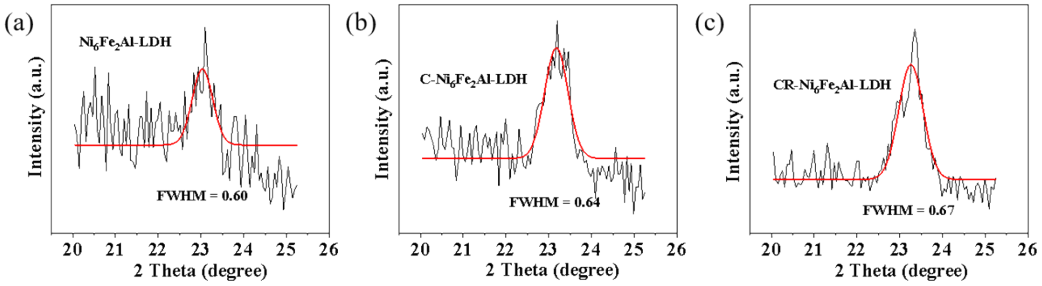

Fig. S6. The full-width half-maximum of the diffraction peaks at 22.9° of (a) Ni_6Fe_2Al-LDH. (b) C-Ni_6Fe_2Al-LDH. (c) CR-Ni_6Fe_2Al-LDH.

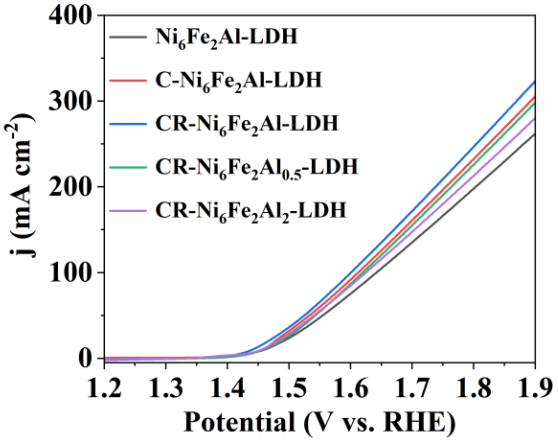

Fig. S7. LSV curves of Ni_6Fe_2Al-LDH, C-Ni_6Fe_2Al-LDH, CR-Ni_6Fe_2Alx-LDH (x= 1, 0.5 and 2) without iR compensation.

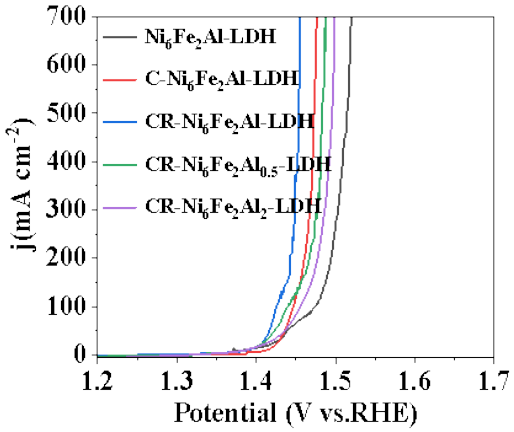

Fig. S8. The LSV curves measured with forward scanning direction from 0.17 V to 0.6 V (vs. Hg / HgO) at a scan rate of 5 mV s^{-1}.

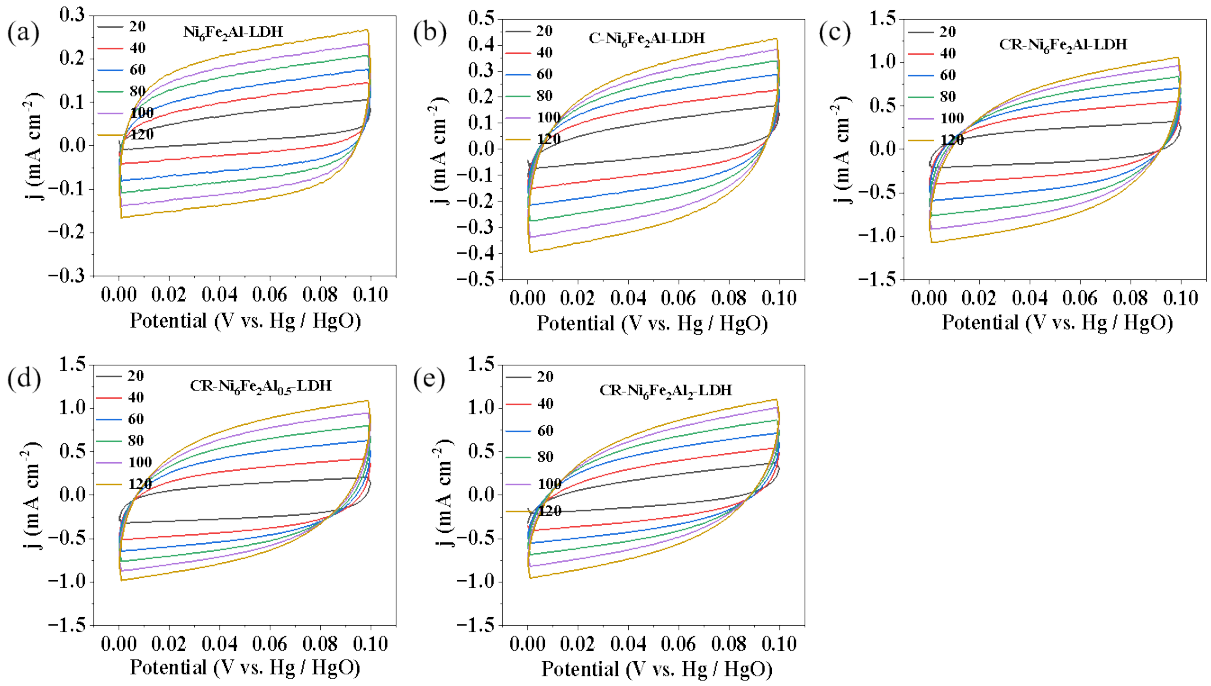

Fig. S9. Typical cyclic voltammograms at different scan rates of prepared samples. (a) Ni_6Fe_2Al-LDH. (b) C-Ni_6Fe_2Al-LDH. (c) CR-Ni_6Fe_2Al-LDH. (d) CR-$Ni_6Fe_2Al_{0.5}$-LDH. (e) CR-$Ni_6Fe_2Al_2$-LDH.

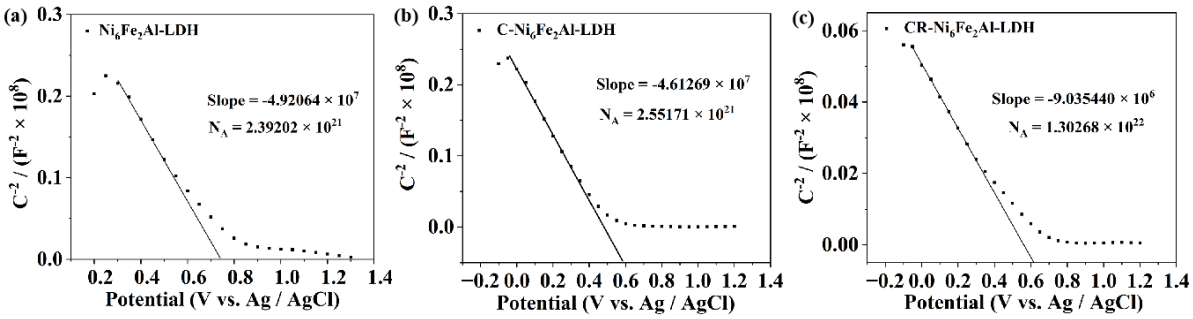

Fig. S10. Mott-Schottky plots of prepared samples. (a) Ni_6Fe_2Al-LDH. (b) C-Ni_6Fe_2Al-LDH. (c) CR-Ni_6Fe_2Al-LDH.

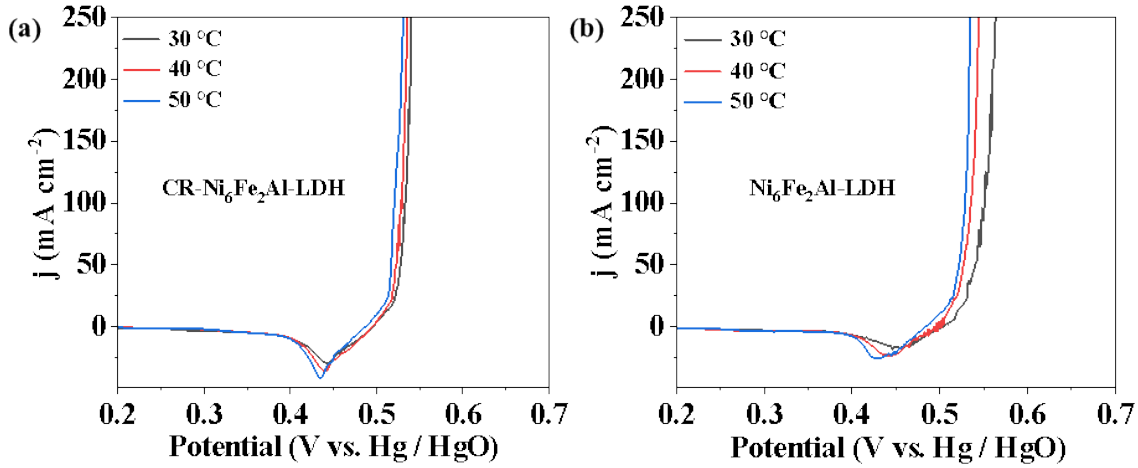

Fig. S11. LSV curves toward OER at different temperature of prepared samples. (a) Ni_6Fe_2Al-LDH. (b) CR-Ni_6Fe_2Al-LDH.

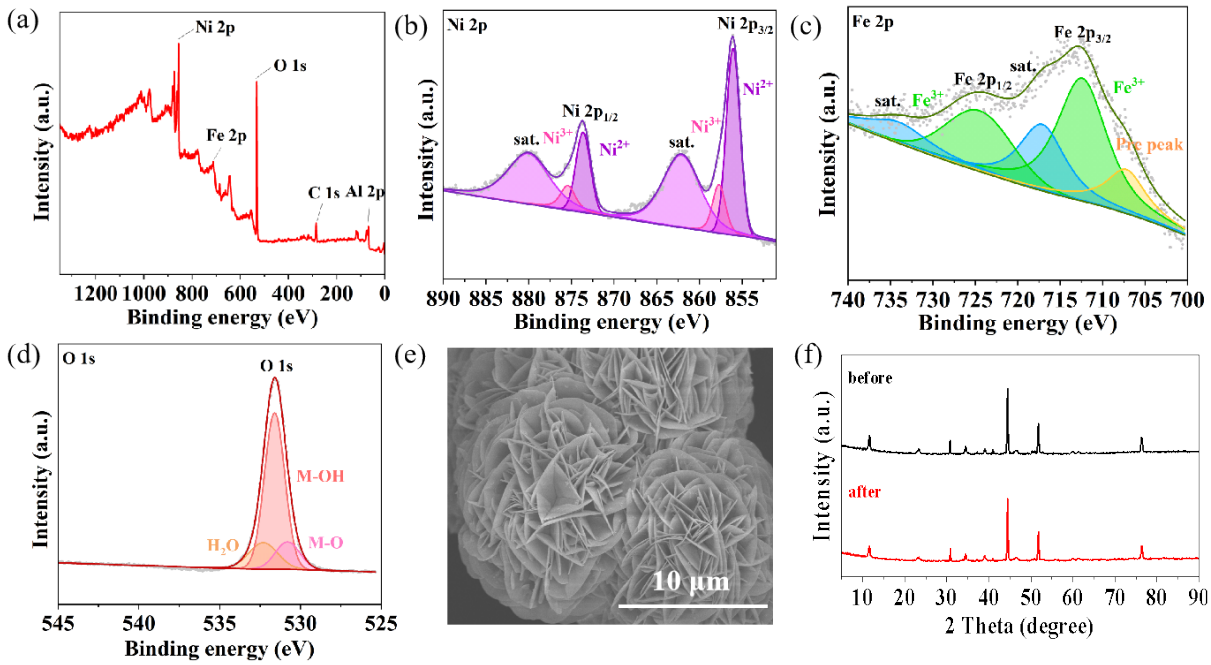

Fig. S12. XPS spectra and XRD patterns of prepared samples after stability test. (a-f) XPS survey spectrum (a), Ni 2p (b), Fe 2p (c), O 1s XPS data (d), SEM image (e) and XRD (f) of CR-Ni_6Fe_2Al-LDH.

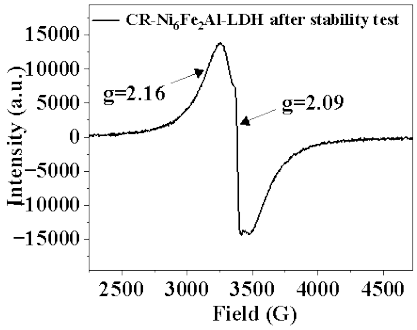

Fig. S13. The ESR spectra of CR-Ni_6Fe_2Al-LDH after stability test.

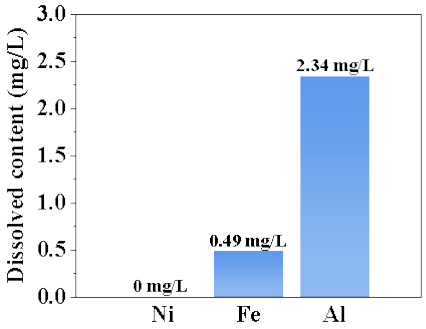

Fig. S14. The dissolved content of Ni, Fe, Al in KOH after stability test determined by ICP-OES measurement.

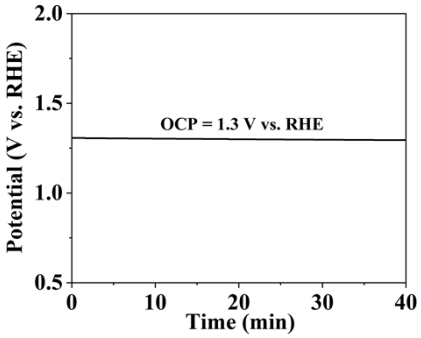

Fig. S15. The open circuit potential curve of the prepared sample.

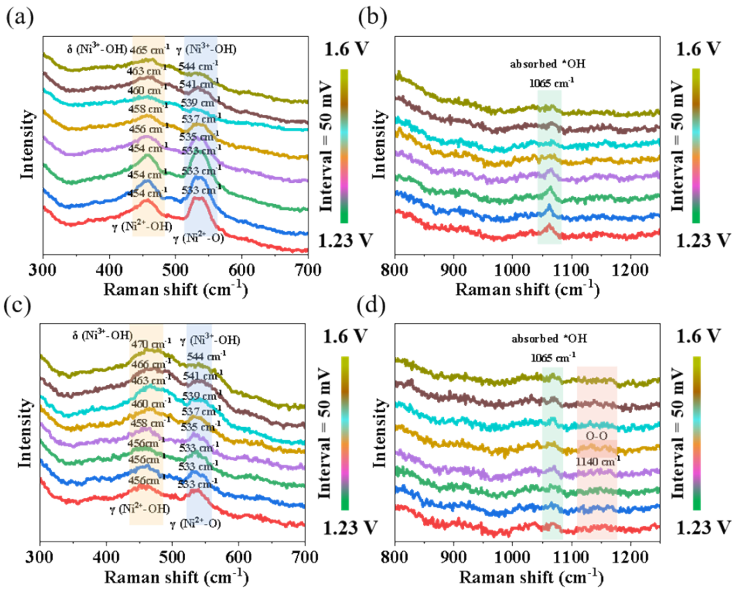

Fig. S16. OER Raman spectra in 1 mol L^{-1} KOH of prepared samples. (a, b) Ni_6Fe_2Al-LDH. (c, d) CR-Ni_6Fe_2Al-LDH.

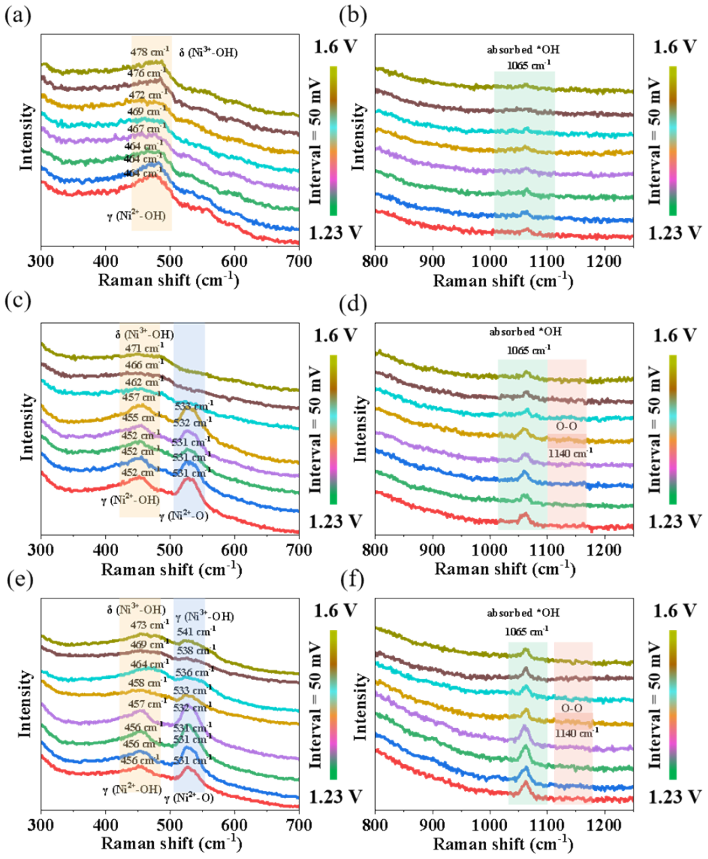

Fig. S17. OER Raman spectra in 1 mol L^{-1} KOH of prepared samples. (a, b) C-Ni_6Fe_2Al-LDH. (c, d) CR-$Ni_6Fe_2Al_{0.5}$-LDH. (e, f) CR-$Ni_6Fe_2Al_2$-LDH.

Table S1. The calculated peak area ratio of M-OH/M-O in Ni_6Fe_2Al-LDH, C-Ni_6Fe_2Al-LDH, CR-Ni_6Fe_2Al-LDH, CR-$Ni_6Fe_2Al_{0.5}$-LDH and CR-$Ni_6Fe_2Al_2$-LDH.

Material	M-OH/M-O
Ni_6Fe_2Al-LDH	4.50
C-Ni_6Fe_2Al-LDH	5.30
CR-Ni_6Fe_2Al-LDH	8.00
CR-$Ni_6Fe_2Al_{0.5}$-LDH	6.12
CR-$Ni_6Fe_2Al_2$-LDH	5.62

Table S2. Catalytic performance of CR-Ni_6Fe_2Al-LDH and some reported LDHs for OER.

Electrocatalyst	Overpotential/current (mV/mA cm^{-2})	Tafel slope (mV dec^{-1})	Electrolyte	Refs
CR-Ni_6Fe_2Al-LDH	223/500	16.3	1M KOH	**This work**
cd-NiFe LDH-$NaBH_4$	205/10	31.1	1M KOH	[1]
D-NiMnLDH/FeS	184/10	49	1M KOH	[2]
D-NiFeAl-LDHs/NF	207/10	34	1M KOH	[3]
NiFe-LDH-Vo@NiCu	244/50	51.2	1M KOH	[4]
$Ni_{0.3}Fe_{0.7}$-LDH@NF	184/10	56.68	1M KOH	[5]
d-(Fe, Ni)OOH	300/500	44	1 M KOH	[6]
NiFeCe-LDH@CP	232/10	31.69	1M KOH	[7]
Co_1Fe_3-LDHs-Vo	253/50	26.8	1M KOH	[8]
Mo-NiCo LDHs(Vo)	258/10	94.5	1M KOH	[9]
v-NiFe LDH	195/10	47.9	1M KOH	[10]
NiFe-LDH-NSs/NF	170/10	39.3	1M KOH	[11]
NiCo LDH-V_{Ni}/CC	227/10	67	1M KOH	[12]
O_{v2}-NiFe hydroxide	214/10	43	1M KOH	[13]
IrO_2@SL-NiFe LDHs	270/10	59	1M KOH	[14]
Co, Mo-NiFe LDH	255/100	43	1M KOH	[15]
HE-LDHs-V^+/CC	227/10	41.2	1M KOH	[16]

Table S3. Comparison of kinetic parameters of OER in alkaline media at 25 ℃ for Ni_6Fe_2Al-LDH, C-Ni_6Fe_2Al-LDH, CR-$Ni_6Fe_2Al_x$-LDH and some reported electrocatalysts.

Material	b/mV dec^{-1}	η_{10}/mV	Source
CR-Ni_6Fe_2Al-LDH	16.3	189	**This work**
C-Ni_6Fe_2Al-LDH	17.4	198	**This work**
CR-$Ni_6Fe_2Al_{0.5}$-LDH	17.6	213	**This work**
CR-$Ni_6Fe_2Al_2$-LDH	19.1	214	**This work**
Ni_6Fe_2Al-LDH	20.6	216	**This work**
3CNT/CNF-240C	19.4	280	[17]
CNF-SO_4	33.8	231	[18]
cobalt PCP	28	361	[19]
NiCo/Fe_3O_4/MOF-74	29	238	[20]
CoVFeN@NF	34.8	212	[21]

Table S4. R_{ct} and R_s of Ni_6Fe_2Al-LDH, C-Ni_6Fe_2Al-LDH, CR-Ni_6Fe_2Al-LDH, CR-$Ni_6Fe_2Al_{0.5}$-LDH and CR-$Ni_6Fe_2Al_2$-LDH.

Material	R_{ct} [Ω]	R_s [Ω]
Ni_6Fe_2Al-LDH	0.47	1.41
C-Ni_6Fe_2Al-LDH	0.34	1.32
CR-Ni_6Fe_2Al-LDH	0.32	1.22
CR-$Ni_6Fe_2Al_{0.5}$-LDH	0.36	1.26
CR-$Ni_6Fe_2Al_2$-LDH	0.51	1.37

Table S5. $\varepsilon_{O\ 2p}$ and $\varepsilon_{Ni\ 3d}$ of Ni_6Fe_2Al-LDH, C-Ni_6Fe_2Al-LDH and CR-Ni_6Fe_2Al-LDH.

Material	$\varepsilon_{O\ 2p}$ [eV]	$\varepsilon_{Ni\ 3d}$ [eV]
Ni_6Fe_2Al-LDH	-4.68	-2.18
C-Ni_6Fe_2Al-LDH	-3.90	-1.85
CR-Ni_6Fe_2Al-LDH	-1.86	-1.57

References

1. X. Li, Y. Liu, Q. Sun, Z. Huangfu, W.-H. Huang, Z. Wang, C.-C. Chueh, C.-L. Chen and Z. Zhu, ACS Sustainable Chem. Eng., 2022, **10**, 14474−14485.
2. M. Sun and J. Wang, J Mater. Chem. A, 2023, **11**, 21420−21428.
3. T. Wang, M. Guo, X. Zhang, Y. Cao, Q. Wu, J. Tu and K. Zhang, ACS Appl. Nano Mater., 2023, **6**, 6002−6010.
4. H. Su, J. Jiang, N. Li, Y. Gao and L. Ge, Chem. Eng. J., 2022, **446**, 137226.
5. Y. Zhai, X. Ren, Y. Sun, D. Li, B. Wang and S. Liu, Appl. Catal. B: Environ., 2023, **323**, 122091.
6. L. Wu, M. Ning, X. Xing, Y. Wang, F. Zhang, G. Gao, S. Song, D. Wang, C. Yuan, L. Yu, J. Bao, S. Chen and Z. Ren, Adv. Mater., 2023, **35**, 2306097.
7. Y. Liao, R. He, W. Pan, Y. Li, Y. Wang, J. Li and Y. Li, Chem. Eng. J., 2023, **464**, 142669.
8. H. Li, C. Tian, L. Wang, Y. Mo, J. Li, C. Wang, C. Li, L. Zheng, F. Huang and Q. Li, Today Energy, 2023, **35**, 101307.
9. K. Chen, Y.-H. Cao, S. Yadav, G.-C. Kim, Z. Han, W. Wang, W.-J. Zhang, V. Dao and I.-H. Lee, Chem. Eng. J., 2023, **463**, 142396.
10. S. Liu, H. Zhang, E. Hu, T. Zhu, C. Zhou, Y. Huang, M. Ling, X. Gao and Z. Lin, J. Mater. Chem. A, 2021, **9**, 23697−23702.
11. Z. Zhao, Q. Shao, J. Xue, B. Huang, Z. Niu, H. Gu, X. Huang and J. Lang, Nano Res., 2022, **15**, 310–316.
12. W. He, D. Cao, D. Ma, Y. Li, C. Chen, L. Liang and H. Liu, Chem. Commun., 2022, **58**, 7757–7760.
13. K. Wu, L. Shi, Z. Wang, Y. Zhu, X. Tong, W. He, J. Wang, L. Zheng, Y. Kang, W. Shan, Z. Wang, A. Huang and B. Jiang, Chem. Commun., 2023, **59**, 3138–3141.
14. D. Li, T. Li, G. Hao, W. Guo, S. Chen, G. Liu, J. Li and Q. Zhao, Chem. Eng. J., 2020, **399**, 125738.
15. Y. Zhao, Q. Wen, D. Huang, C. Jiao, Y. Liu, Y. Liu, J. Fang, M. Sun and L. Yu, Adv. Energy Mater., 2023, **13**, 2203595.
16. J. Yao, F. Wang, W. He, Y. Li, L. Liang, Q. Hao and H. Liu, Chem. Commun., 2023, **59**,

3719–3722.

17. Y. Qi, Z. Yang, S. Peng, Y. Dong, M. Wang, X.-Q. Bao, H. Li and D. Xiong, Inorg. Chem. Front., 2022, **9**, 332.
18. R. Zhang, L. Wang, L. Pan, Z. Chen, W. Jia, X. Zhang and J.-J. Zou, Appl. Catal. B: Environ., 2020, **277**, 119237.
19. J. Kang, M. J. Lee, N. G. Oh, J. Shin, S. J. Kwon, H. Chun, S.-J. Kim, H. Yun, H. Jo, K. M. Ok and J. Do, Chem. Mater., 2021, **33**, 2804–2813.
20. X. Wang, H. Xiao, A. Li, Z. Li, S. Liu, Q. Zhang, Y. Gong, L. Zheng, Y. Zhu, C. Chen, D. Wang, Q. Peng, L. Gu, X. Han, J. Li and Y. Li, J. Am. Chem. Soc., 2018, **140**, 15336–15341.
21. D. Liu, H. Ai, J. Li, M. Fang, M. Chen, D. Liu, X. Du, P. Zhou, F. Li, K. H. Lo, Y. Tang, S. Chen, L. Wang, G. Xing and H. Pan, Adv. Energy Mater., 2020, **10**, 2002464.